

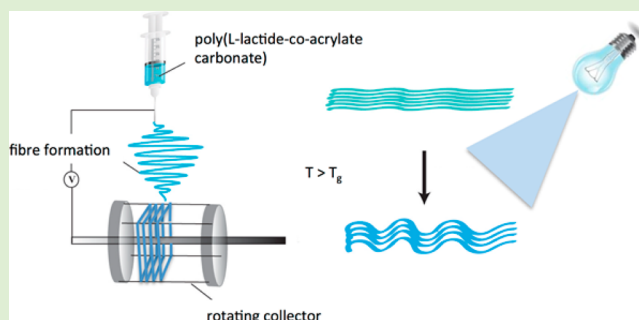
Electrospun Poly(L-lactide-co-acryloyl carbonate) Fiber Scaffolds With a Mechanically Stable Crimp Structure For Ligament Tissue Engineering

Fei Chen, James W. S. Hayami, and Brian G. Amsden*

Department of Chemical Engineering and Human Mobility Research Centre, Queen's University, Kingston, Canada

S Supporting Information

ABSTRACT: The aim of this study was to prepare a fibrous scaffold that possesses a crimped morphology using a photo-cross-linkable biodegradable copolymer. To obtain the crimped morphology, the polymer was first electrospun onto a rotating wire mandrel to obtain aligned straight fibers. Postprocessing by immersion in aqueous buffer at 37 °C generated a crimplike pattern in the fibers. It was reasoned that cross-linking the fibers following formation of the crimped structure would endow the scaffolds with a recoverable crimp pattern and mechanical properties similar to that of the collagen fibers in the anterior cruciate ligament (ACL). To achieve this aim, a trimethylene carbonate based monomer bearing an acrylate pendant group was synthesized and copolymerized with L-lactide. The copolymer was electrospun and photo-cross-linked yielding fibrous scaffolds possessing a substantial increase in tensile modulus and crimp stability compared to the uncross-linked fibrous scaffolds. The crimp-stabilized scaffolds also showed good cytocompatibility toward 3T3 fibroblasts, which attached and grew along the crimped fibers. These findings suggest that these cross-linked fiber scaffolds may be useful for the generation of cultured ligament tissue.



1. INTRODUCTION

The anterior cruciate ligament (ACL) is the most frequently injured ligament of the knee. The ACL does not heal effectively when torn, likely as a result of the washing away of any blood clot that begins to form by the synovial fluid that surrounds the ligament. Without a clot to form a provisional matrix and stabilize the torn ends of the ACL, cells cannot regenerate the damaged tissue.¹ Suture repair of the ACL has been ineffective with over 90% of the patients treated in that manner failing to heal.^{2,3} The afflicted knee joint cannot support the same loads, and if the ligament is left untreated, subsequent chondral and meniscal injury, and early osteoarthritis, may result.⁴ For these reasons, surgical reconstruction of the ACL is often required.

The current dominant reconstruction strategy is to implant autograft tendon tissue. Although generally successful, conversion of the autograft to ligamentous tissue is a long process and has the disadvantages of anterior knee pain, decreased range of motion, donor site morbidity, and limited donor tendon availability.^{4,5} The limitations of these existing ACL replacement approaches have led to the investigation of tissue-engineered ligament grafts.^{6–12}

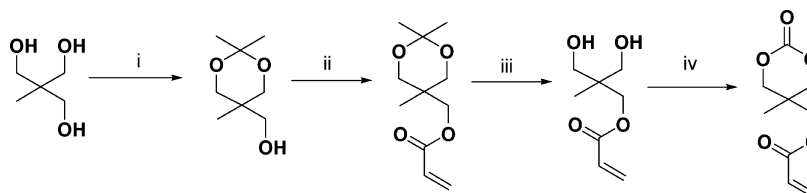
However, to date no engineered ACL tissue has the appropriate extracellular architecture or mechanical properties following *in vivo* transplantation. This is due in large part to the lack of scaffolds with adequate structure and mechanical properties capable of supporting ligament development *in vitro* and remodeling *in vivo*. During the remodeling stage of healing

under *in vivo* conditions, the extracellular matrix formed is a disorganized, hypercellular tissue having a different crimp pattern than is present normally.¹³ As a result, the healing tissue has reduced mechanical strength.¹³ Therefore, a clinically acceptable engineered ACL tissue should possess biological architecture and mechanical properties closely aligned with native ACL to allow for physiologic loading after implantation. In the human ACL, fibroblasts within the extracellular matrix secrete collagen molecules that then self-assemble sequentially into microfibrils, fibrils, and fibers (1–32 μm in diameter).^{14,15} The fibrils are cross-linked to each other, forming fiber bundles called fascicles (100–250 μm in diameter).^{14,15} The fibers are aligned along the long axis of the ligament and display a wavelike pattern along their length called crimp.^{14–16} This crimp pattern repeats every 45–60 μm .¹⁶ Crimp plays a biomechanical role at both the cellular and tissue level.^{14,15} The ACL is characterized by a bimodal stress–strain response with a compliant response referred to as the toe region at low strains, which changes to a stiff response at larger strains.^{17,18} The crimp pattern allows for 7 to 16% of creep before permanent deformation and ligament damage occurs.¹⁵ Larger loads then elongate the fibers causing a gradual increase in tissue stiffness.^{15,19} The established standard mechanical properties

Received: December 10, 2013

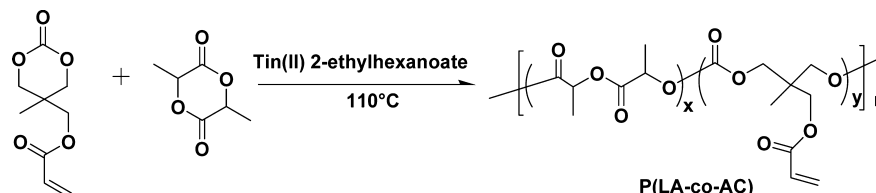
Revised: April 2, 2014

Published: April 3, 2014

Scheme 1. Four-Step Synthesis Process for the Preparation of the AC Monomer^{24a}

^aReaction conditions: (i) tris(hydroxymethyl)ethane, *p*-toluenesulfonic acid monohydrate, acetone, room temperature; (ii) acryloyl chloride, triethylamine, tetrahydrofuran, 0 °C; (iii) HCl (1.0 M), methanol, room temperature; (iv) ethyl chloroformate, triethylamine, tetrahydrofuran, 0 °C. Reproduced from ref 24. Copyright 2009 American Chemical Society.

Scheme 2. Ring-Opening Polymerization of LLA with the AC Monomer and Final Copolymer Structure



of the human ACL from young donors are a Young's modulus of 111 MPa,²⁰ ultimate tensile strength of 38 MPa,²⁰ and 12 N·m for energy absorbed at failure.¹⁷

We have recently developed an electrospinning technique that generates nano/micro polymer fibers that are aligned. These fibers spontaneously crimp when immersed in 37 °C phosphate-buffered saline.²¹ Scaffolds prepared from these fibers also exhibit a toe region when pulled in uniaxial tension.^{21,22} We have also demonstrated that a crimp pattern in scaffolds is beneficial in that fibroblasts seeded on such scaffolds and cultured under dynamic stretching conditions produced an extracellular matrix (ECM) approximating the composition of native ACL and formed fascicle-like collagen bundles, whereas fibroblasts seeded on linear fibers did not.²² This response was reasoned to be due to the approximation of the deformation conditions normally experienced by an ACL fibroblast attached to the collagen fiber. While these results are promising, the copolymer that has been used to date, poly(L-lactide-*co*-D,L-lactide) did not possess adequate mechanical properties when hydrated (Young's modulus of ~10 MPa), lost its crimp pattern under long-term dynamic stimulation, and exhibited modest fibroblast attachment.²³

The primary objective of this study was to improve on this scaffold design by altering the polymer composition. It was reasoned that cross-linked fibrous scaffolds would maintain fiber crimp structure upon dynamic loading and result in significantly increased hydrated scaffold modulus. To produce a cross-linkable polymer fiber, a trimethylene carbonate based monomer bearing an acryloyl pendant group (5-methyl-2-oxo-1,3-dioxan-5-yl acrylate, or acryloyl carbonate for simplicity) was synthesized (Scheme 1) and copolymerized with L-lactide (Scheme 2). The acryloyl carbonate (AC) monomer was chosen as it can be easily copolymerized with other lactone monomers and can be readily cross-linked through radical polymerization initiated for example by UV irradiation. Copolymers were synthesized containing different amounts of AC monomer, and these copolymers were electrospun into crimped polymer mats, which were subsequently photo-cross-linked. The cross-linked scaffolds were assessed for mechanical properties in uniaxial tension both initially and following *in vitro* degradation under static conditions for their ability to

maintain a toe region and crimped pattern following dynamic loading and for fibroblast adhesion and proliferation.

2. MATERIALS AND METHODS

All materials were used as received unless otherwise noted. Stannous 2-ethylhexanoate (95% purity), and Dulbecco's Modified Eagle's Medium were obtained from Sigma-Aldrich, ON, Canada. L-lactide was obtained from Purac, The Netherlands, and purified by recrystallization from anhydrous toluene. The following were used in the synthesis of the AC monomer: tris(hydroxymethyl)ethane and 2,2-dimethoxypropane (ACROS Organics, New Jersey, U.S.A.), *p*-toluenesulfonic acid monohydrate, acryloyl chloride, and ethyl chloroformate (Sigma-Aldrich, Oakville, ON, Canada), acetone, diethyl ether, potassium carbonate, tetrahydrofuran (THF), triethylamine, methanol, and hydrochloric acid (Fisher Scientific, Canada). THF was dried with 4 Å molecular sieves for 2 days before use.

2.1. Polymer Synthesis. Acryloyl carbonate (AC) was synthesized via a four step process (Scheme 1) based on the synthesis described by Chen et al.²⁴ Once synthesized, the AC monomer was copolymerized with L-lactide (LLA) at varying molar ratio via ring-opening polymerization utilizing stannous 2-ethylhexanoate as a catalyst and octan-1-ol as an initiator (Scheme 2). The copolymerization was carried out in toluene at 110 °C for 24 h. The monomer to initiator mole ratio was set at 500:1, while the initiator to catalyst mole ratio was 300:1. The resulting copolymers were then purified by dissolving in CH₂Cl₂ and precipitating in cold methanol.

2.2. Polymer Characterization. The monomer compositions of the poly(L-lactide-*co*-acryloyl carbonate) (P(LLA-AC)) copolymers were determined from ¹H NMR spectra obtained from a Bruker Avance-400 MHz spectrometer.²⁴ The synthesized copolymers were dissolved in chloroform-*d* (Fluka, Canada) at 10 mg/mL and their chemical shifts were measured relative to the methyl proton resonance of an internal tetramethylsilane reference. The integration of chemical shifts corresponding to ~5.2 ppm (methine hydrogen of LLA groups), and 5.6–6.4 ppm (intact vinyl protons of AC monomer) were used to determine the monomer compositions. A Mettler Toledo DSC1 system was used to measure the thermal properties (glass transition temperature (*T*_g), melting point (*T*_m), and heat of fusion (ΔH_f)) of the synthesized copolymers. The samples were taken through two heating cycles and one cooling cycle. The heating cycles ran from –80 to 180 °C, while the cooling cycle ran from 180 to –80 °C. A 10 °C/min, heating rate with a 3 min hold time at each set point was utilized. The *T*_g was measured from the second heating cycle, while *T*_m and ΔH_f were measured from the first heating cycle. The minimum of the endothermic curve in the first heating cycle was taken as *T*_m, while the

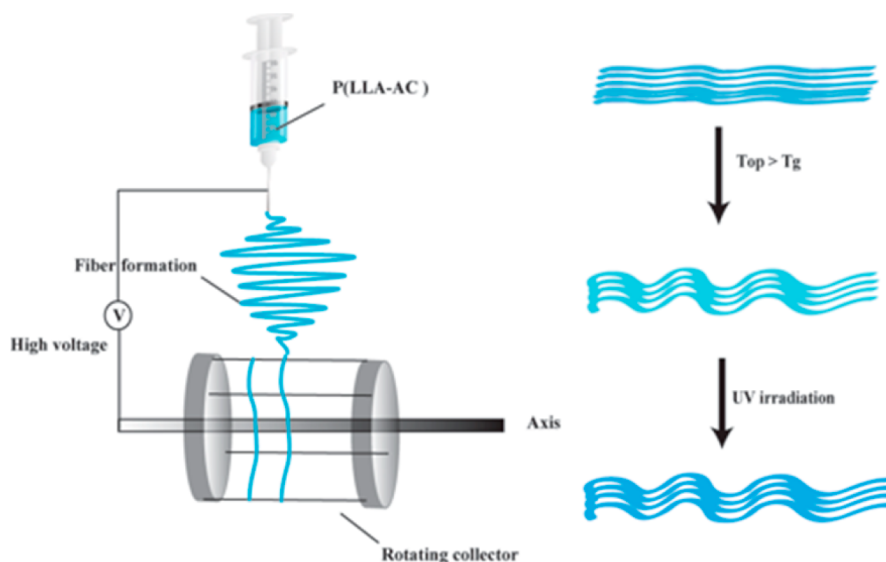


Figure 1. Schematic illustration of the preparation of the crimped and cross-linked fiber scaffolds. T_{op} refers to the operating, or ambient, temperature while T_g refers to the polymer glass transition temperature.

area bound by the endotherm normalized to mass of the polymer sample was used to calculate ΔH_f . The crystallinity of the polymers was calculated by dividing the measured ΔH_f value by the ΔH_f of purely crystalline poly(L-lactide) (93.1 J/g^{25}). The number-average molecular weight (M_n), weight-average molecular weight (M_w), and molar-mass dispersity (D_M) were measured using a Viscotek 270max Separation Module equipped with a refractive index (RI) detector. A set of two porous PolyAnalytik columns with an exclusion limit molecular weight of $20 \times 10^6 \text{ g/mol}$ were used in series. The calibration curve based on the RI detector was constructed using narrow molecular weight poly(styrene) standards ranging from 6910 to 844 000 g/mol. THF at 40°C was used as the mobile phase at a flow rate of 1 mL/min with the polymer sample dissolved in THF at concentration of 10 mg/mL. Results were analyzed and fitted in Astra v4.90.07 software (Wyatt Technology, U.S.A.).

2.3. Fabrication of Crimped and Photo-Cross-Linked Fibrous Scaffolds. The copolymers were electrospun into fibers as described previously.²¹ In this process, the polymers were dissolved in a 3:1 (volume ratio) solution of dichloromethane/dimethylformamide (DCM/DMF) (Sigma-Aldrich Ltd., Canada) at a concentration ranging from 20 to 35% (w/v). The electrospinning apparatus consisted of a syringe pump (KD Scientific Inc., U.S.A.), high voltage generator (Gamma Voltage Research, U.S.A.) and a rotating wire mandrel (collection device) (Figure 1). The wire mandrel was constructed using two circular end pieces of 5 cm diameter that were connected by four equally spaced, 10 cm long connecting rods. The wire mandrel was attached to a horizontally mounted in-line mixer (Barnant, Series 20, U.S.A.), which rotated at 1000 rpm (as measured with a contact tachometer, Exttech). The polymer solutions were pumped at a flow rate of 0.03 mL/min through a 21 ga. blunt tip needle (Becton Dickinson & Company, U.S.A.). The air gap between the needle tip and ground plate was set at 15 cm, and a 1 kV/cm positive electric field was applied between the air gap using the voltage generator. Electrospinning was performed at ambient conditions (relative humidity 50–70% and $20\text{--}22^\circ\text{C}$). The fibers collected on the wire mandrel were stored at room temperature in a vacuum desiccator until required. The aligned fibers were cut from the mandrel and immersed in phosphate buffered saline (PBS) at 37°C for 30 min to induce a crimped pattern and to remove trace amounts of residual DMF. The resultant crimped fibers were then divided into two groups. One group of fibers were photo-cross-linked for 5 min per side in their wet state using a UV light source (EFOS 3000, EXFO Canada) at an intensity and wavelength of 100 mW cm^{-2} and 365 nm, respectively. The second group of fibers was left uncross-linked as controls.

2.4. Characterization of P(LLA-AC) Fibrous Scaffolds. Fiber diameter and crimp parameters were measured from SEM images. The fiber mats were air-dried, mounted on aluminum stubs, pulse sputter coated (Anatech Hummer VI-A Sputter Coater, U.S.A.) and imaged with a JEOL JSM840 SEM (Peabody, Japan) with HKL Flamenco EBSD data acquisition software (version 5.0.6.0, U.S.A.). The alignment of the fibers was manually quantified from the SEM images using ImageJ, by measuring the orientation angles relative to the horizontal for a minimum of 100 fibers. Fiber diameter ($n = 100$) and crimp parameters (wavelength and amplitude, $n = 20$) were determined from SEM images processed with Sigma Scan Pro that was calibrated for each magnification with the in-image scale. The mechanical properties of the crimped electrospun fiber mats were measured in uniaxial tension at 37°C using a micromechanical tester (Mach-1, Biomomentum, Canada), to determine the change in material properties with respect to the change in AC content (3, 5, 8, and 12 mol %) for dry scaffolds, and during in vitro degradation in PBS for scaffolds prepared with the copolymer containing 12 mol % AC (0, 1, 3, and 5 weeks). For the week 0 value, the scaffolds were immersed in PBS for 30 min to become hydrated prior to measuring the mechanical properties. For these measurements, rectangular fiber scaffolds were cut from the mandrel in the direction of the fiber alignment and were transferred onto cardboard windows using double-sided adhesive tape (Scotch, 3M Canada). The ends of the window were mounted between the grips of the Mach-1, the sides of the cardboard window cut with scissors, and the scaffolds pulled at a rate of 1% strain/s until failure with load and displacement captured at 100 Hz. Tensile stress in the fibers was calculated as the measured force normalized to the total cross sectional area of the fibers mounted in the sample, as described in Surrao et al.²³ The applied strain was measured as the deformation normalized to the gauge length of the scaffold sample. The modulus of the crimped fiber scaffolds was determined from a linear regression of the linear region of the stress-strain curve. The equilibrium water uptake of the polymers was determined by soaking the fibrous scaffolds in PBS for 24 h at 37°C ($n = 3$). Following soaking, the scaffolds were dabbed dry with a Kimwipe and weighed, then dried in vacuo (15 mmHg, 20°C) for 48 h and weighed again. The water content of the hydrated fibers is reported as the difference in wet versus dry weight of the scaffolds divided by the initial dry weight of the scaffolds.

To determine the ability of the crimp to be recovered for uncross-linked and cross-linked fiber scaffolds prepared with P(LLA-AC) of 12% AC content, the initial gauge length of the fiber scaffolds (measured from the exposed fibers between the edges of the mounting frame) was used to set the gage distance of the micromechanical tester

Table 1. Physical Properties of P(LLA-AC) Copolymers before and after Cross-Linking

mol % AC in feed	product mol % AC	M_n (kDa)	D_M	uncross-linked			cross-linked			
				T_g^a (°C)	T_m^a (°C)	X_c (%)	T_g^a (°C)	T_m^a (°C)	X_c (%)	%w/w water ^b
3	2	72.1	1.2	58	161	31	63	143	4	8 ± 5
6	5	62.2	1.1	56	156	32	64	137	4	11 ± 5
10	8	55.9	1.2	55	154	22	65	135	3	12 ± 6
20	12	61.5	1.2	50	147	26	67	124	5	9 ± 7

^a $n = 2$, standard deviations are ±1 °C. ^bHydrated water content, equilibrium value measured at 24 h for the electrospun scaffolds, $n = 3$.

grips. The mounting frame was placed in the grips so that none of the frame edges were exposed to ensure no slack was present in the fiber mats prior to testing. The immediate load profile during testing also indicated there was no slack in the mounted scaffolds (no preload was applied). The scaffolds were then pulled to 20% strain at a strain rate of 1%/s. The scaffolds were removed and placed in PBS at 37 °C for 30 min to allow the crimp pattern to recover. The recovered scaffolds were then remeasured for gauge length, which was used to calculate the new 20% total strain and 1%/s strain rate before mounting the scaffolds in the grips at the required zero strain gauge length. This process was continued for a total of 10 pulls unless the scaffold broke. The modulus was calculated from the initial linear slope of the stress versus strain curve for each measurement, which occurred below 10% strain, as described above.

Dynamic testing of crimped fiber scaffolds prepared with P(LLA-AC) of 12% AC content was performed to determine the loading profiles of the scaffolds under rapid loading and unloading conditions at 37 °C. The scaffolds were mounted in the micromechanical tester as described above and were pulled to 10 and 20% strain at 1 Hz for 10 cycles. The loading data were fitted and plotted together to show the progression of the loading curves through the 10 cycles.

Sol content of cross-linked P(LLA-AC) fiber scaffolds was measured by weight loss. The initial dry weights (dry mass_{initial}) were measured using a balance (AT-250 Balance, Mettler Instrument Corporation, U.S.A.), the scaffolds were placed in glass vials containing 5 mL of DCM, and the DCM was replaced every 2 h over a two day period. At the end of day 2, the scaffolds were vacuum-dried overnight in an oven set at 37 °C, and the dry mass (dry mass_{final}) measured. The sol content of the scaffolds was calculated using

$$\text{Sol content} = \frac{\text{dry mass}_{\text{initial}} - \text{dry mass}_{\text{final}}}{\text{dry mass}_{\text{initial}}}$$

2.5. Cell Culture. NIH 3T3 fibroblasts were maintained in Dulbecco's Modified Eagle's Medium (DMEM, Sigma-Aldrich, Canada) supplemented with 10% fetal bovine serum (FBS Sigma-Aldrich, Canada) and 1% antibiotic in a 37 °C and 5% CO₂ incubator between passage P1 and P4 before seeding on the fiber scaffolds. Discs (8 mm dia.) were cut from the fiber scaffolds using a disposable biopsy punch and sterilized by UV light exposure for 30 min per side in a laminar flow hood and then placed in a 24 well culture plate. Cells were seeded onto one side of the scaffolds at a density of 2.5×10^4 cells/scaffold using a seeding volume of 50 μ L. The cells were allowed to attach for 4 h and then 1.95 mL of supplemented medium was added. The medium was replaced after 2 days. The number of metabolically active cells was measured using the MTT assay 24 and 72 h after seeding.

2.6. Statistics. Measured values are presented as the average ± the standard deviation about the average with the number of replicate samples indicated by n . Statistical differences were assessed using a one-way Kruskal–Wallis or two-way Friedman analysis of variance with a Bonferroni posthoc test using $p < 0.05$ as a measure of significance.

3. RESULTS AND DISCUSSION

3.1. Synthesis of the AC monomer. The functional cyclic carbonate monomer AC was synthesized in four steps according to Chen et al.²⁴ Moderate total yields of about

40% were obtained. A representative ¹H NMR spectrum obtained in CDCl₃ of the synthesized AC monomer as well as the peak assignments are provided in Supporting Information Figure 1.

3.2. Synthesis of P(LLA-AC). The aim of this study was to provide a versatile approach to synthesizing photo-cross-linkable polymers with similar mechanical properties to the ACL. On the basis of our previous findings, wherein poly(L-lactide-co-D,L-lactide) (80:20 L-lactide/D,L-lactide molar ratio) fiber scaffolds exhibited modulus values of approximately 10 MPa in the hydrated state,²³ L-lactide was chosen as the predominant monomer and copolymerized with AC. The resultant copolymers had a high molecular weight and moderate molar-mass dispersity (1.2–1.5), as measured by GPC (Table 1). Importantly, the ¹H NMR spectra of the copolymers clearly displayed chemical shifts at 5.6–6.4 ppm, attributable to intact vinyl protons on the pendant acryloyl group (Figure 2). The composition of the copolymers was

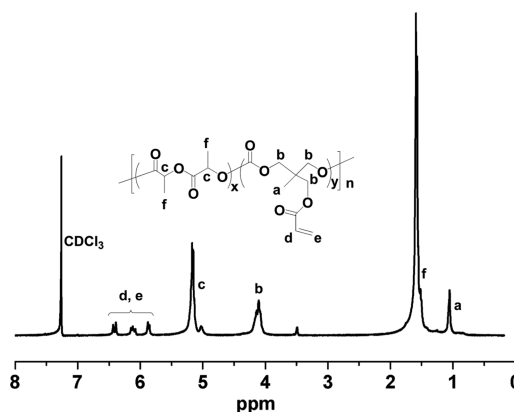


Figure 2. Representative ¹H NMR spectrum of the P(LLA-AC)(12% AC) copolymer.

determined by comparing the integrals of signals of the acryloyl vinyl protons with those of PLLA methine protons at $\delta = 5.16$ ppm. It was evident that both functionality and molecular weight of copolymers of AC and LLA could be readily controlled using the polymerization technique employed. However, it must be noted that when a high feed ratio of AC monomer (20%) was used in the copolymerization, only 12–14% AC was present in the resulting copolymer (Table 1). The relatively low AC incorporated into the copolymer structure is believed to be due to a lower reactivity of the AC monomer compared to LLA, likely as a result of the bulky pendant acryloyl group.²⁶ A similar result was reported by Chen et al.²⁴

The number-average molecular weight (M_n), molar-mass dispersity (D_M), and thermal properties of the synthesized copolymers are also listed in Table 1. A single glass transition temperature (T_g) was detected on the first and second heating

cycles for all the copolymers. The T_g , melting point (T_m), and degree of crystallinity (X_c) of the copolymers tended to decrease with increasing AC monomer content due to AC monomer insertion into the copolymer backbone resulting in disruption of the regular close packing of molecular chains. Following cross-linking, the T_g tended to increase for all the copolymers and was roughly the same for each at approximately 65 °C. The melting point and degree of crystallinity also tended to decrease for each copolymer. The melting points of the cross-linked samples again tended to decrease with increasing AC content in the copolymer, while the degree of crystallinity was substantially reduced and was approximately equivalent for each network at ~4%. These results are expected for a cross-linked copolymer, as cross-linking restricts polymer chain movement and interferes with the ability of the LLA blocks along the backbone to align and crystallize.²⁷

Following incubation in PBS at 37 °C for 24 h, cross-linked fiber scaffolds of the copolymers absorbed statistically equivalent amounts of water ($p = 0.12-0.58$), circa 10 w/w %, indicating that notable hydration of the polymer occurs before substantial degradation of the polymer begins and that the extent of hydration is unaffected by the relatively low amounts of AC monomer incorporated into the copolymer. Further, the cross-linked polymer fibers had relatively low sol contents (from 16 to 6%) that decreased as the AC monomer content of the polymer increased (Table 2), indicating that the cross-linking efficiency increased with an increase in available pendant acryloyl groups.

Table 2. Sol Contents of the Cross-Linked P(LLA-AC) copolymers^a

copolymer	sol content (%)
P(LLA-AC)(5%AC)	16.5 ± 0.2
P(LLA-AC)(8%AC)	11.3 ± 0.5
P(LLA-AC)(12%AC)	6.25 ± 0.2

^a($n = 3$).

3.3. Fabrication of Fibrous P(LLA-AC) Scaffolds. Defect free P(LLA-AC) fibers with smooth edges were obtained. The diameter of the fibers ($n = 100$) was measured from SEM images (Figure 3). The rotating mandrel used to collect the fibers produced aligned microfibers; 85% of the fibers were within $\pm 10^\circ$ from the horizontal. The average diameter of the

electrospun P(LLA-AC) fibers were $0.9 \pm 0.12 \mu\text{m}$ (Table 3). The aligned fibers were effectively treated to possess a crimp

Table 3. Crimp Parameters and Average Diameter of the P(LLA-AC) Fibers^a

copolymer	fiber diameter (μm)	crimp parameters	
		wavelength (μm)	amplitude (μm)
P(LLA-AC)(5%AC)	0.9 ± 0.24	44 ± 13	28 ± 9
P(LLA-AC)(8%AC)	0.72 ± 0.12	49 ± 6	31 ± 5
P(LLA-AC)(12%AC)	0.85 ± 0.10	42 ± 9	22 ± 5

^a $n = 100$ for fiber diameters and $n = 20$ for crimp parameters.

pattern (Figure 3), yielding crimp amplitudes and wavelengths similar to those of the collagen fibers present in native ACL (amplitude of 5–10 μm , and wavelength of 45–60 μm , respectively¹⁶).

3.4. Uniaxial Tensile Measurement of Fiber Scaffolds' Mechanical Properties. The Young's moduli of the cross-linked scaffolds, measured before immersion in water, are presented in Figure 4. Although the scaffolds consisting of

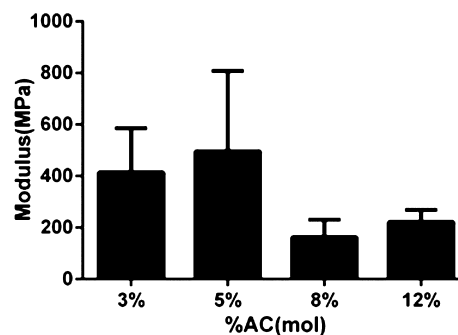


Figure 4. Cross-linked scaffold Young's modulus with respect to the mol % AC monomer in the copolymer. ($n = 4$).

copolymers prepared with lower molar amounts of AC monomer (3 and 5%) exhibited greater average moduli than those with 8 and 12% AC, these measurements had greater variability and there was no significant differences between the Young's moduli of the scaffolds in the dry state. Each dry scaffold measured had a Young's modulus greater than that of

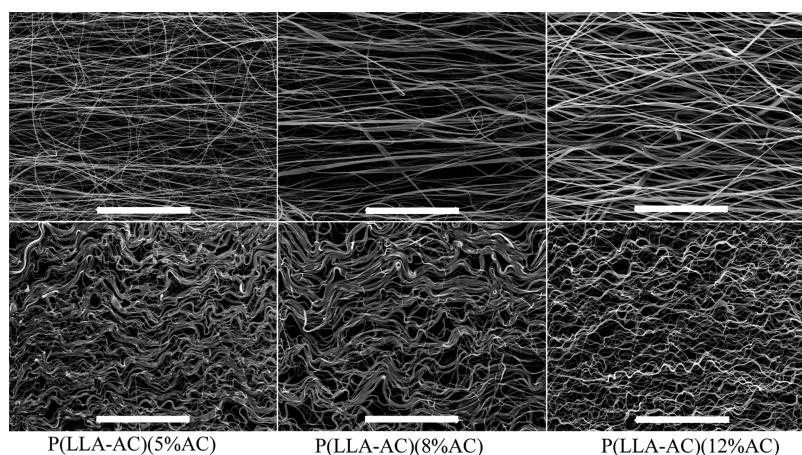


Figure 3. SEM images of electrospun P(LLA-AC) fibers before and after crimping (scale bar 200 μm).

the target value of 110 MPa. Given that the scaffolds prepared with the copolymer possessing 12% AC monomer had the lowest sol content and the least degree of variability in its modulus values, these scaffolds were chosen for further assessment.

Cross-linking the P(LLA-AC)(12%AC) scaffolds had an obvious improvement on the modulus of the scaffolds (Figure 5). The modulus of the dry, cross-linked scaffolds ($222 \text{ MPa} \pm$

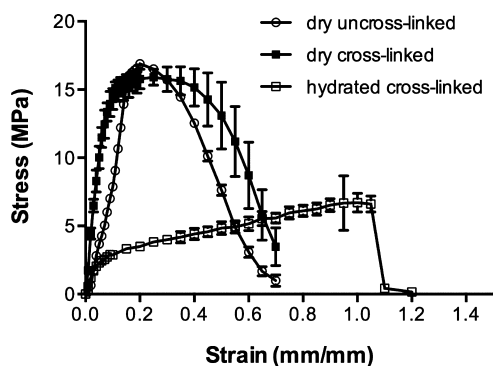


Figure 5. Stress–strain curves of dry P(LLA-AC)(12%AC) fiber scaffolds before and after cross-linking and hydrated cross-linked fiber scaffolds. The average modulus of the dry uncross-linked fiber scaffolds was $86 \pm 5 \text{ MPa}$ and that of the dry cross-linked scaffolds was $222 \pm 28 \text{ MPa}$. The average modulus of the hydrated scaffolds was $26 \pm 1.4 \text{ MPa}$. ($n = 3$).

28) was almost two times higher than that of the uncross-linked scaffolds ($86 \pm 5 \text{ MPa}$). Furthermore, the cross-linked scaffolds displayed an obvious plateau region between the yield point and the final break point. This plateau region is probably due to an interconnected molecular entanglement structure in the cross-linked sample. Once hydrated, the modulus of the fiber scaffolds decreased to $26 \pm 1.4 \text{ MPa}$, and a plateau region was no longer observed. Instead, the fibrous scaffolds exhibited rubbery behavior with a lower ultimate tensile strength and an increased elongation at break. This behavior can be attributed to a plasticization effect²⁸ due to absorbed water.²³

3.5. Dynamic Mechanical Properties of Hydrated 88:12 P(LLA-AC) Scaffolds. The P(LLA-AC)(12%AC) scaffolds were subjected to dynamic loading and a pull-relaxation test following hydration in pH 7.4 buffer. The hydrated condition was necessary to reflect the future performance of the scaffolds within a dynamically stimulated bioreactor. Repetitive crimp unfolding of the photo-cross-linked P(LLA-AC) fibers over 10 loading cycles demonstrated a further advantage of cross-linking the polymer following crimp induction. The cross-linked scaffolds exhibited a nearly linear initial loading profile (Figure 6), while a pronounced toe region was observed for each following loading cycle. The change in loading profile was due possibly to fiber breakage and/or release of interfiber entanglements. Following the first loading cycle, a reproducible loading profile was observed for the 10 cycles tested. The length of the toe region was dependent on the ultimate strain applied; with an ultimate applied strain of 10%, the toe region was approximately 4%, while with an ultimate applied strain of 20% the toe region was approximately 10%. The difference in the length of the toe region could be due to the difference in the overall strain applied coupled with the time allowed for the fibers to relax and recover their initial crimped pattern, or the differences in the strain rates applied.

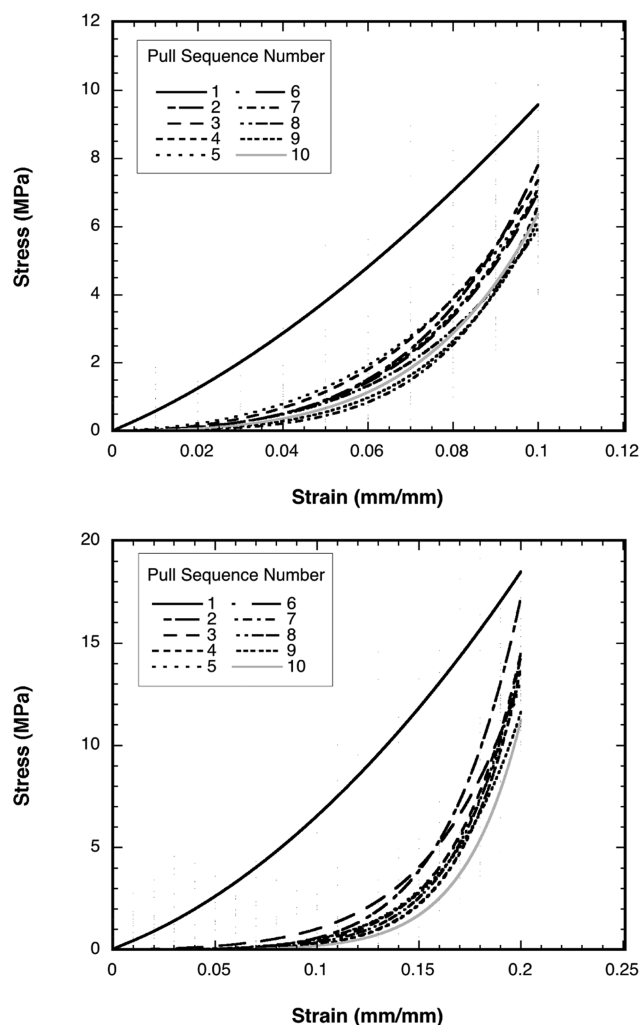


Figure 6. Stress–strain response of the hydrated and cross-linked fiber scaffolds following dynamic loading. Conditions: 1 Hz for 10 cycles. Top: up to 10% strain. Bottom: up to 20% strain. The lines represent curve fits to the data. ($n = 3$).

To further confirm the recoverability of the crimp pattern following uniaxial extension induced by photo-cross-linking, the change in the gauge length (which is a measure of the degree of crimp unfolding under applied strain) and modulus of the scaffolds were measured following a series of pull-relaxation cycles. Differences between pulls and between cross-linked versus uncross-linked were assessed using a two-way Friedman analysis of variance. There was a slight, but not significant, downward trend in modulus of the cross-linked scaffolds over 10 pull-relaxation cycles (Figure 7A), which remained at approximately $30.1 \pm 10 \text{ MPa}$. In contrast, a continuous and significant decrease in modulus when compared to the initial modulus for uncross-linked scaffolds was observed from pull-relaxation cycles 3–6. Following pull 6, only one scaffold remained unbroken. The modulus of this scaffold stayed constant at approximately 10 MPa for the remaining pulls. Moreover, the gauge length increased with each pull-relaxation cycle for the uncross-linked scaffolds, whereas the gauge length of cross-linked scaffolds remained constant (Figure 7B).

The crimp pattern of the photo-cross-linked P(LLA-AC) fibers after 10 pull-relaxation cycles was examined visually from SEM images (Figure 8). These images clearly show that the crimped and cross-linked fibers recovered their initial wave-

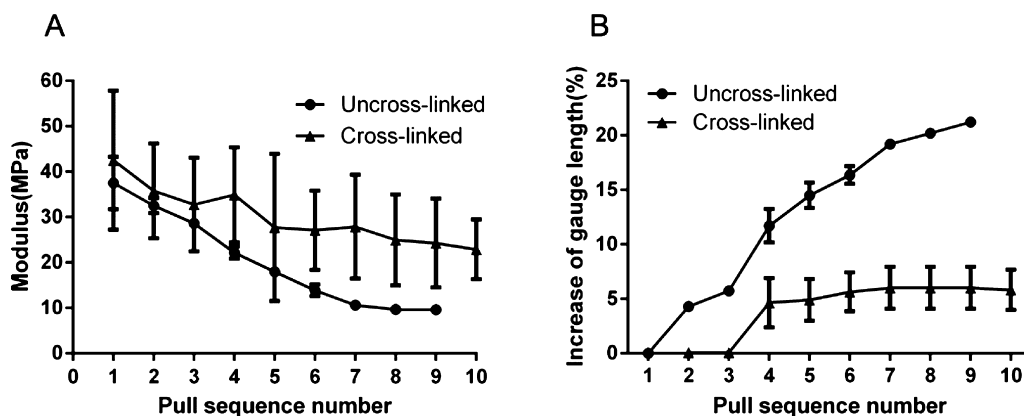


Figure 7. Change in (A) modulus and (B) recoverable gauge length following a series of pull-relaxation cycles for both uncross-linked and cross-linked hydrated P(LLA-AC)(12AC%) scaffolds. Conditions: 1 Hz for 5 cycles, up to 20% strain. Relaxation condition: immersed in 37 °C water for 30 min. ($n = 3$).

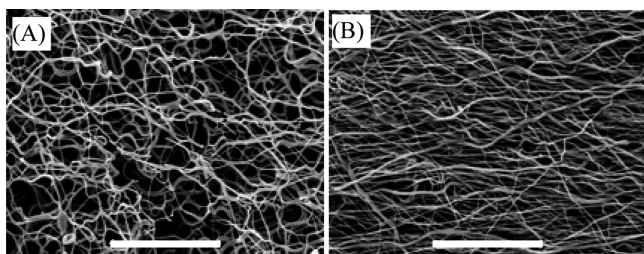


Figure 8. SEM images of P(LLA-AC)(12%AC) fibers following 10 cycles of pulling-relaxation: (A) cross-linked, (B) uncross-linked (scale bar 200 μm).

length and amplitude after the scaffolds were allowed to rest in an aqueous environment at 37 °C, while uncross-linked fibers had lost a notable degree of their original crimp structure.

3.6. Change in Properties of P(LLA-AC)(12%AC) Scaffolds during in Vitro Degradation. The fiber scaffolds used in this experiment possessed an initial modulus of approximately 26 ± 1.4 MPa in the wet state (Table 4), which

Table 4. Mechanical and Thermal Properties of Cross-Linked P(LLA-AC)(12%AC) Fibre Scaffolds Following in Vitro Degradation

time (week)	modulus (MPa)	T_g - first heating cycle (°C)	T_g -second heating cycle (°C)
0	26 ± 1.4	41	55
1	21 ± 4.0	40	55
3	18 ± 3.5	38	53
5	21 ± 5.2	37	54

^a $n = 3$ for modulus and $n = 2$ for thermal properties, for every time point. The pooled standard deviation of the glass transition values is ± 1 .

is consistent with the results reported above in Figure 7, and significantly greater than that obtained previously (10 ± 4 MPa²³) for scaffolds composed of crimped, but uncross-linked, poly(L-lactide-co-D,L-lactide) fibers. The explanation for the reduction in modulus of the fiber scaffolds upon hydration being due to plasticization of the network by the absorption of water provided above is supported by the observed difference between the T_g of the hydrated sample (T_g from the first heating cycle) and that of the dry sample (T_g from the second heating cycle) (Table 4). There was no significant drop in the

modulus of the cross-linked fiber scaffolds throughout the degradation study time period. The copolymer exhibited a slight decrease in T_g at 5 weeks when compared to the initial T_g , indicative of the onset of polymer degradation. To determine whether there were any changes in fiber structure during the in vitro degradation, SEM images from each time point were taken. Figure 9 shows the morphology of the

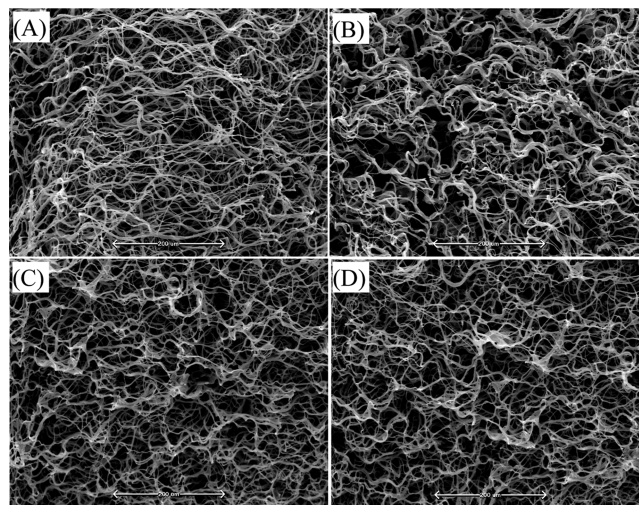


Figure 9. SEM micrographs of cross-linked P(LLA-AC)(12%AC) fiber scaffolds incubated in 1× PBS at 37 °C showing that the crimp structure in the fibers is retained over the period studied: (A) week 0, (B) week 1, (C) week 3, and (D) week 5 (scale bar 200 μm).

scaffolds of each degradation time points. There were no obvious differences before and after incubation within the aqueous medium, such as no evidence of surface pitting or broken fibers, demonstrating that the crimped structure parameters were unaffected by long-term incubation in an aqueous environment under static conditions.

3.7. Fibroblast Attachment and Proliferation on Cross-Linked P(LLA-AC) Scaffolds. To determine whether the AC content of the copolymer had any effect on cell attachment and proliferation, 3T3 fibroblasts were seeded on uncross-linked and cross-linked fiber scaffolds prepared using copolymers with 3, 5, 8, and 12 mol % AC. While not relevant for an assessment of the potential of the scaffolds for the generation of ligament tissue, 3T3 fibroblasts are a standard cell

line used for the assessment of biomaterial cytotoxicity.²⁹ The MTT assay was used to assess cell number on the scaffolds, based on a measurement of the metabolic activity of the cells at 24 and 72 h (Figure 10A). The data is normalized to the metabolic activity of fibroblasts seeded onto TCPS at the same seeding density in Figures 10B,C.

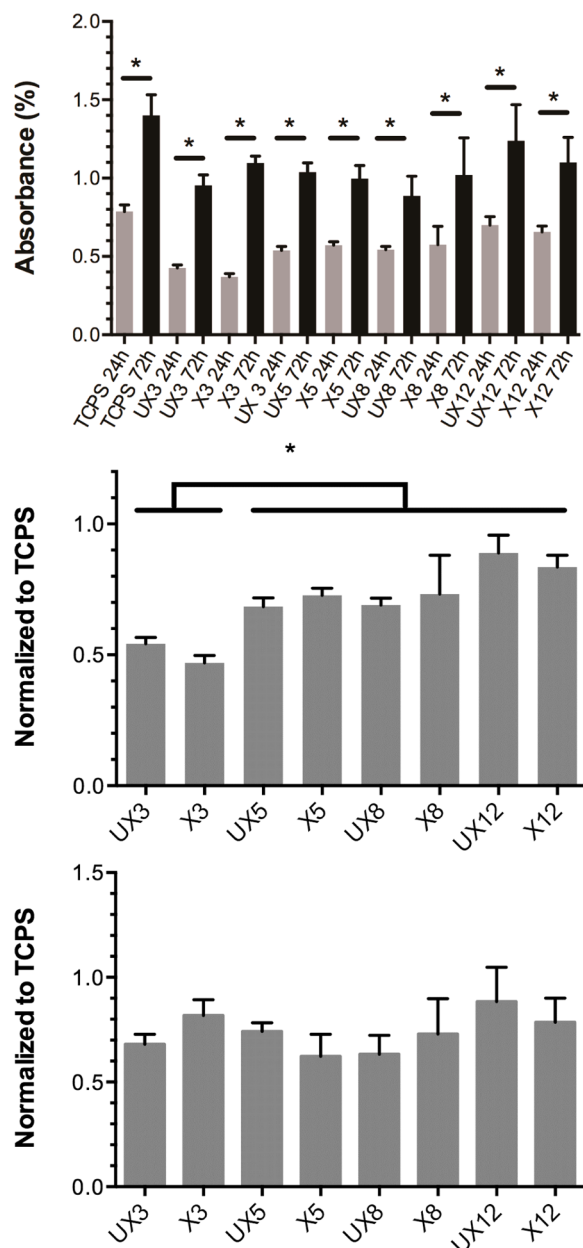


Figure 10. (A) 3T3 fibroblast number following seeding on uncross-linked (UX) cross-linked (X) fiber scaffolds prepared with copolymers of varying mol % AC (number following X or UX), as assessed with the MTT assay (top) and normalized to cell number on TCPS controls at 24 h (middle) and 72 h (bottom) ($n = 3$, *: $p < 0.05$).

There was a significant difference between 24 and 72 h absorbances for each scaffold (Figure 10A). This result confirms that the 3T3 fibroblasts were able to attach and proliferate on these scaffolds. After 24 h, except for scaffolds prepared with P(LLA-AC)(12%), there were fewer fibroblasts on the scaffolds than on the TCPS controls (Figure 10B). There was no difference between the cell number on the cross-

linked versus uncross-linked scaffolds prepared with P(LLA-AC) of the same AC content, regardless of the AC content of the polymer, suggesting that the presence of the pendant acrylate group on the polymer was not cytotoxic. Fewer fibroblasts attached to the scaffolds prepared with P(LLA-AC) (3%) than on the scaffolds prepared with P(LLA-AC) of higher AC content (5–12% AC), for which there was no significant difference with respect to AC content. It is possible that the higher lactide content of the 3% AC polymers produced a different protein deposition profile on these polymer fiber surfaces with fewer fibroblast adhesion sites exposed for effective attachment. At 72 h, there were no significant differences between the cell numbers on any of the scaffolds or the TCPS controls; however, the cell numbers on the scaffolds tended to be lower than on the TCPS controls (Figure 10C). SEM images (Figure 11) confirmed that the 3T3 fibroblasts attached to the cross-linked fibers and were aligning along the fiber long axes by 24 h and were proliferating.

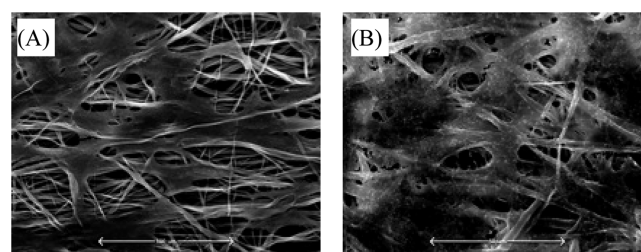


Figure 11. SEM images of 3T3 fibroblasts on cross-linked P(LLA-AC)(12% AC) scaffolds (A) 24 h and (B) 72 h after seeding (scale bar 100 (left) and 50 μm (right)).

CONCLUSIONS

Previous work by our group has demonstrated that scaffolds possessing a crimped architecture similar to that of the native anterior cruciate ligament are beneficial in terms of the rate and composition of extracellular matrix produced by seeded fibroblasts when grown under dynamic loading conditions in a bioreactor. A limitation of the polymers used to date for preparing these scaffolds is that this crimped structure is gradually lost under dynamic mechanical loading. Copolymerizing an acryloyl carbonate monomer with L-lactide yielded a copolymer with an acryloyl pendant group along its backbone that was effectively utilized to cross-link electrospun microfibers possessing an appropriate crimp structure. The cross-linked and crimped fiber scaffolds had a Young's modulus approximating that of the modulus of human anterior cruciate ligaments. Importantly, cross-linking provided a means of stabilizing the fiber crimp structure following dynamic mechanical loading. The crimp structure was also unaffected by static incubation in PBS for up to 5 weeks; nevertheless, the stability of the crimp needs to be assessed under dynamic conditions in buffer in future studies. Finally, fibroblasts seeded onto these fibers effectively attached and proliferated. Collectively, these results demonstrate that this scaffolding approach has potential for the in vitro generation of replacement ligaments.

ASSOCIATED CONTENT

Supporting Information

A representative ^1H NMR spectrum of the synthesized AC monomer is provided, confirming the structure as well as

demonstrating it was free of impurities. This material is available free of charge via the Internet at <http://pubs.acs.org>.

AUTHOR INFORMATION

Notes

The authors declare no competing financial interest.

ACKNOWLEDGMENTS

Funding for this project was provided by the Canadian Institutes of Health Research and the Natural Sciences and Engineering Research Council of Canada (CREATE Bio-interfaces Training Program, CREATE Training Program in Bone and Joint Health Technologies).

REFERENCES

- (1) Murray, M. M.; Fleming, B. C. *J. Orthop. Res.* **2013**, *31*, 1501–1506.
- (2) Feagin, J. A.; Curl, W. W. *Am. J. Sport Med.* **1976**, *4*, 95–100.
- (3) Engebretsen, L.; Benum, P.; Fasting, O.; Mølster, A.; Strand, T. *Am. J. Sport Med.* **1990**, *18*, 585–590.
- (4) Petrigliano, F. A.; McAllister, D. R.; Wu, B. M. *Arthroscopy* **2006**, *22*, 441–451.
- (5) Laurencin, C.; Freeman, J. *Biomaterials* **2005**, *26*, 7530–7536.
- (6) Barber, J. G.; Handorf, A. M.; Allee, T. J.; Li, W.-J. *Tissue Eng., Part A* **2013**, *19*, 1265–1274.
- (7) Little, D.; Guilak, F.; Ruch, D. S. *Tissue Eng., Part A* **2010**, *16*, 2307–2319.
- (8) Kew, S. J.; Gwynne, J. H.; Enea, D.; Abu-Rub, M.; Pandit, A.; Zeugolis, D.; Brooks, R. A.; Rushton, N.; Best, S. M.; Cameron, R. E. *Acta Biomater.* **2011**, *7*, 3237–3247.
- (9) Hayami, J. W. S.; Surrao, D. C.; Waldman, S. D.; Amsden, B. G. *J. Biomed. Mater. Res., Part A* **2010**, *92*, 1407–1420.
- (10) Vaquette, C.; Kahn, C.; Frochot, C.; Nouvel, C.; Six, J.-L.; De Isla, N.; Luo, L.-H.; Cooper-White, J.; Rahouadj, R.; Wang, X. *J. Biomed. Mater. Res., Part A* **2010**, *94A*, 1270–1282.
- (11) Cooper, J. A.; Sahota, J. S.; Gorum, W. J.; Carter, J.; Doty, S. B.; Laurencin, C. T. *Proc. Natl. Acad. Sci. U.S.A.* **2007**, *104*, 3049–3054.
- (12) Bourke, S.; Kohn, J.; Dunn, M. *Tissue Eng.* **2004**, *10*, 43–52.
- (13) Frank, C.; Woo, S.; Amiel, D.; Harwood, F.; Gomez, M.; Akeson, W. *Am. J. Sports Med.* **1983**, *11*, 379–389.
- (14) Frank, C.; Shrive, N.; Lo, I.; Hart, D.; Buckwalter, J.; Einhorn, T.; Simon, S. In *Orthopaedic Basic Science Foundation of Clinical Practice*; American Academy of Orthopaedic Surgeons: Rosemont, IL, 2007.
- (15) Vunjak-Novakovic, G.; Altman, G.; Horan, R. *Annu. Rev. Biomed. Eng.* **2004**, *6*, 131–156.
- (16) Amiel, D.; Billings, E.; Akeson, W. H. In *Knee ligaments structure, function, injury, and repair*; Daniel, D., Akeson, W. H., O'Connor, J. J., Eds.; Raven Press: New York, 1990; pp 77–94.
- (17) Woo, S.; Hollis, J. M.; Adams, D. J.; Lyon, R. M.; Takai, S. *Am. J. Sport Med.* **1991**, *19*, 217–225.
- (18) Jones, R. S.; Nawana, N. S.; Percy, M. J.; Learmonth, D. J. A.; Bickerstaff, D. R.; Costi, J. J.; Paterson, R. S. *Clin. Biomech.* **1995**, *10*, 339–344.
- (19) Woo, S.; Abramowitch, S.; Kilger, R.; Liang, R. *J. Biomech.* **2006**, *39*, 1.
- (20) Noyes, F. R.; Grood, E. S. *J. Bone Joint Surg. Am.* **1976**, *58*, 1074–1082.
- (21) Surrao, D. C.; Hayami, J. W. S.; Waldman, S. D.; Amsden, B. G. *Biomacromolecules* **2010**, *11*, 3624–3629.
- (22) Surrao, D. C.; Fan, J. C. Y.; Waldman, S. D.; Amsden, B. G. *Acta Biomater.* **2012**, *8*, 3704–3713.
- (23) Surrao, D. C.; Waldman, S. D.; Amsden, B. G. *Acta Biomater.* **2012**, *8*, 3997–4006.
- (24) Chen, W.; Yang, H.; Wang, R.; Cheng, R.; Meng, F.; Wei, W.; Zhong, Z. *Macromolecules* **2010**, *43*, 201–207.
- (25) Fischer, E. W.; Sterzel, H. J.; Wegner, G. *Kolloid-Z. Z. Polym.* **1973**, *251*, 980–990.
- (26) Matsuo, J.; Aoki, K.; Sanda, F.; Endo, T. *Macromolecules* **1998**, *31*, 4432–4438.
- (27) Sperling, L. *Introduction To Physical Polymer Science*; John Wiley and Sons: New York, 1992.
- (28) Labrecque, L. V.; Kumar, R. A.; Dave, V.; Gross, R. A.; McCarthy, S. P. *J. Appl. Polym. Sci.* **1997**, *66*, 1507–1513.
- (29) von Recum, A. *Handbook of Biomaterials Evaluation*, 2nd ed.; CRC Press: Boca Raton, FL, 1999; pp 275–289.